



Past, present and future of atomic clocks for GNSS

Bernardo Jadaszliwer¹ · James Camparo¹

Received: 7 August 2020 / Accepted: 20 November 2020 / Published online: 3 January 2021
© Springer-Verlag GmbH Germany, part of Springer Nature 2021

Abstract

Global Navigation Satellite Systems (GNSS) are enabled by atomic clocks, which provide the timing precision and accuracy required for the ranging measurements. Significant investments have been made and will continue to be made, to improve GNSS atomic clock technology and reduce the signal-in-space user range error. After providing a baseline by reviewing current GNSS satellite atomic clock technology, we discuss how far, and in what directions, atomic clock technology should be pushed to provide maximum benefits to GNSS performance, reliability and cost.

Keywords GNSS · Atomic clocks · GPS · Galileo · BeiDou · GLONASS · PNT · Satellite timekeeping

Introduction

All current Global Navigation Satellite Systems (GNSS) have a similar architecture, pioneered by the designers of the US Air Force Global Positioning System (GPS) (Hoffman-Wellenhof et al. 1993). At its most basic level, a constellation of satellites large enough to provide global coverage constantly transmits messages that enable the user's receiver to determine its distance to four or more satellites by measuring signal propagation times. The navigation messages provide the user's receiver with the time and frequency offsets of the satellite clocks from their nominal values, as well as their linear frequency drift rates, thus enabling the virtual synchronization of the constellation clocks. The messages also provide the user's receiver with satellite ephemeris, and from those data the receiver can estimate the user's three-dimensional location and the time offset of his or her local clock from UTC. Satellite clock and ephemeris parameters are updated periodically by the GNSS Ground Control.

The positioning precision and accuracy will depend on the ranging precision and accuracy, which in turn will depend on the precision and accuracy of the ephemeris data and the onboard clocks. It is easy to see that for any practical GNSS concept of operations, the requirements for onboard timekeeping precision and accuracy can only be met

by atomic clocks. The typical frequency precision of high-performance ovenized crystal oscillators (OCXO) roughly 24 h after update is of the order of a few parts in 10^{11} . Let us assume that the GNSS concept of operations requires updating clock frequency and time every 24 h, as is the case with GPS (Hoffman-Wellenhof et al. 1993). A very good space-qualified OCXO will have a 24-h frequency stability of 2×10^{-11} (even after ignoring frequency drift), resulting in a 24-h timekeeping uncertainty of 1.7×10^{-6} s, and a ranging uncertainty of about 500 m, leading to positioning uncertainties of the same order of magnitude. To reduce those uncertainties to a level of about 5 m, the GNSS concept of operations would require hourly updating of the satellite clocks. In practice, this requirement would necessitate a very extensive, complex GNSS ground control segment or an extensively cross-linked GNSS constellation.

An additional problem with the possible use of OCXOs as GNSS satellite clocks is presented by their intrinsic radiation sensitivity. While frequency drift caused by exposure to the space radiation environment can be monitored and compensated with appropriate clock updates, rapid frequency and phase changes caused by events such as large solar flares cannot be detected and compensated promptly enough, causing large increases to user range error, as dramatically illustrated on July 14, 2000, by an event remembered as “the Bastille Day solar flare.” The Milstar communication system satellites fly rubidium (Rb) atomic clocks, except for the first one flown into orbit which carried only high-quality crystal oscillators, with the active OCXO slaved via cross-link time transfer to an atomic clock flying on another Milstar satellite

✉ James Camparo
james.c.camparo@aero.org

¹ Physical Sciences Laboratories, The Aerospace Corporation, El Segundo, CA, USA

(Camparo et al. 1997). On July 14, 2000, a large solar flare occurred, increasing the number of high-energy solar protons in the vicinity of the Earth by four orders of magnitude. This caused a radiation-induced 10^{-10} jump in the OCXO frequency that, if left uncorrected for 24 h, would have caused a 10^{-5} s time error. Fortunately, the OCXO on Milstar Flight-1 was slaved via cross-links to a Rb atomic clock having a very low radiation sensitivity, as is the case with all atomic clocks, and so the corrected Flight-1 clock displayed less than a 2.7×10^{-7} s total time discontinuity (Camparo et al. 2004). Since 2000, additional radiation-induced jumps in this OCXO's frequency have been observed, displaying a power-law dependence on the flux of solar protons with an energy greater than 50 meV (LaLumondiere et al. 2003).

Those considerations mandate the use of atomic clocks onboard GNSS satellites. The first Navigation Technology Satellite (NTS-1), launched in the summer of 1974, successfully demonstrated operation of a Rb atomic clock in space. The satellite carried two atomic clocks and operated for 5 years (Beard et al. 1986). The success of the NTS-1 atomic clock technology demonstration paved the road for the use of atomic clocks in all GNSS.

Figure 1 shows the three generations of rubidium atomic clocks used on GPS satellites. First on the left is the clock used on GPS I and GPS II/IIA satellites, designed and manufactured by Efratom and modified for space flight by Rockwell, Inc. Next, in center, is the PerkinElmer (now Excelitas) clock used on GPS IIR satellites, displaying much improved performance. And on the right is the Excelitas clock used on GPS IIF satellites (Dupuis et al. 2008), incorporating additional performance-improving modifications. The coffee cup at the center is shown as a size reference.

All current GNSSs are enabled by atomic clocks, which provide the timing precision and accuracy required for the ranging measurements. Significant investments have been made and will continue to be made, to improve GNSS atomic clock technology and reduce the signal-in-space user range error (SIS-URE). In the next section, we will provide

a technology baseline by reviewing atomic clocks currently used on board GNSS satellites.

2020 GNSS satellite clocks

Four distinct GNSS have satellites currently orbiting the earth: the US Global Positioning System (GPS), the Russian Federation Globalnaya Navigazionnaya Sputnikovaya Sistema (GLONASS), the European Union's Galileo system and the People's Republic of China's BeiDou system.

GPS satellites fly cesium (Cs) and Rb atomic clocks (Vannicola et al. 2010); GLONASS satellites (Revniykh 2016) fly Cs and Rb atomic clocks, with plans to fly passive Hydrogen masers; Galileo satellites fly Rb clocks and passive H-masers (Maciuk 2019), and BeiDou satellites fly Rb clocks and passive H-masers (Lv et al. 2018). From the point of view of a GNSS systems engineer, the desirability of a particular atomic clock technology is determined by the careful consideration of three distinct aspects: its time-keeping performance, its reliability and operational life, and its size, weight and power requirements, usually captured together under the acronym "SWaP." Alas, this typically means that none of those characteristics can be optimized by itself, but a balanced compromise between all three must be reached, with different compromises based on different system requirements.

All the atomic clocks currently used on board GNSS satellites have a similar architecture: A local oscillator (typically a high performance, space-qualified OCXO) is frequency-locked to an atomic hyperfine transition frequency (Major 1998). The clock physics package allows the local oscillator to interrogate the reference atomic transition frequency and generates a correction signal that constantly drives the local oscillator frequency (typically, after multiplication by a factor of the order 10^3) toward the atom's resonant frequency. Hyperfine transitions are chosen as the frequency references for GNSS atomic clocks because their

Fig. 1 Still life with space-qualified rubidium atomic clocks and an Aerospace Corporation-logged coffee cup. From left to right: Efratom/Rockwell GPS I, II and IIA atomic clock; PerkinElmer (now Excelitas) GPS IIR atomic clock; coffee cup; Excelitas GPS IIF atomic clock



frequencies fall in the microwave regime, convenient for practical electronics engineering.

The ground state of H, Rb and Cs atoms is split by the hyperfine interaction into two sublevels (Major 1998). Since the hyperfine splittings are small compared to room temperature thermal energies, both sublevels are equally populated when in thermal equilibrium. Before interrogating the atomic hyperfine transition, a difference in the population of both sublevels must be created; this is achieved in different ways for each one of the aforementioned clock technologies and will be discussed more fully below. However, prior to discussing specific clock technologies we will first briefly review how one characterizes the timekeeping performance of an atomic clock.

Atomic clock performance characterization

The last quarter of a century has witnessed an explosion in the number of different approaches to characterize the frequency stability of an atomic clock, as described by Riley (2008). For our purposes, it will suffice to use the oldest, simplest and most commonly seen of those, the two-sample or Allan variance $\sigma_y^2(\tau)$, where τ is the frequency-averaging time (Riley 2008).

Figure 2 shows a plot of a notional Allan deviation $\sigma_y(\tau)$ displaying the three types of frequency noise commonly found in atomic clocks: white frequency noise, flicker frequency noise and random walk frequency noise. For relatively short averaging times, all atomic clocks routinely display white frequency noise behavior, characterized by a $1/\sqrt{\tau}$ dependence on averaging time. Eventually, “colored” frequency noise behavior, either flicker frequency noise, independent of τ , or random walk frequency noise, proportional to $\sqrt{\tau}$, becomes dominant.

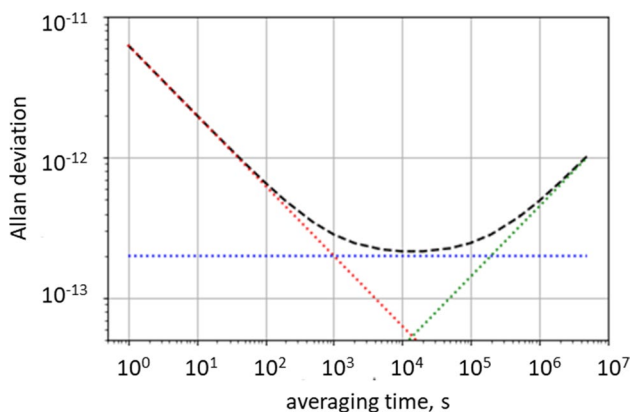


Fig. 2 Allan deviation $\sigma_y(\tau)$ versus averaging time τ . Black dash curve: $\sigma_y(\tau)$ for a notional clock. Red, blue and green dot lines: white, flicker and random walk frequency noise contributions, respectively

The white noise frequency behavior of the clock is often determined by the fundamental physics of the atomic hyperfine transition interrogation and can be predicted to be

$$\sigma_y(\tau) = \frac{\alpha}{Q \times \text{SNR}} \frac{1}{\sqrt{\tau}} = \frac{A}{\sqrt{\tau}} \quad (1)$$

where $Q = \nu_0/\Delta\nu$ is the quality factor of the hyperfine transition line (center frequency ν_0 and full width at half-maximum $\Delta\nu$), SNR is the detection signal-to-noise ratio, and α is a constant of order unity that depends on the details of the interrogation technique. The Heisenberg uncertainty principle dictates that $\Delta\nu$ will be inversely proportional to the length of the atomic interrogation time, which can be defined as the duration of the coherent interaction between the atomic hyperfine states and the microwave field. This can be limited by the residence time of the atoms within the microwave field, or by the time interval between dephasing collisions with background atoms or molecules or container walls.

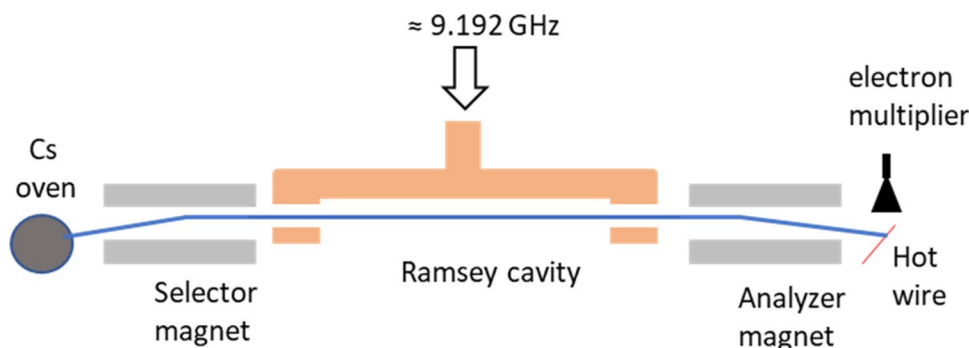
The above result is predicated on the idealization of the interrogation process as a moderate strength microwave field interacting with an isolated, unperturbed atom. Actually, the interrogated atom is constantly interacting with its immediate environment: atomic and molecular collisions, atom/surface collisions, static and near-resonant electromagnetic fields, etc. Those interactions perturb the atomic hyperfine energy levels, and those perturbations cause the hyperfine frequency transition to shift away from its nominal value ν_0 . Fluctuations in the atomic environment thus result in a fluctuating output clock frequency, which manifests itself as clock colored frequency noise.

The art of atomic clock engineering is, thus, to maximize the atomic interrogation time and SNR and to minimize environmental perturbations during interrogation, so as to reduce the colored frequency noise as much as possible and push the transition from white to colored frequency noise out to as long an averaging time as possible.

Cesium atomic clock

A Cs atomic clock or cesium frequency standard (CFS) performs an atomic beam microwave resonance experiment in a package a few tens of centimeters long, using the atomic beams toolkit developed by Rabi and coworkers in the 1930s and 1940s (Ramsey 1956). As illustrated in Fig. 3, a Cs atomic beam is generated in an effusive oven; a uniform gradient state selector magnet deflects atoms in one of the ground-state hyperfine sublevels into a Ramsey-type, separated fields atomic resonance cavity. A second uniform gradient state analyzer magnet, placed after the cavity, deflects atoms that have changed their hyperfine state inside the cavity onto a hot wire ionizer, followed by an electron

Fig. 3 Schematic diagram of a CFS physics package displaying its main elements: Cs oven, state selector and analyzer magnets, separate fields Ramsey cavity and hot wire/electron multiplier Cs atom detector. Not shown are the magnetic shields, the C-field coil and the ion pump, and Cs getters required to keep the physics package under vacuum



multiplier. The multiplier signal will be null in the absence of a near-resonant microwave field in the cavity, and it will peak when the frequency of the microwaves injected into the cavity equals the hyperfine transition frequency for Cs, $\nu_0 \approx 9.2$ GHz, providing the means to lock the microwave frequency to ν_0 .

The atomic interrogation time (and thus the hyperfine transition line Q) is limited by the length of the resonance cavity, and for the compact CFSs on board GNSS satellites, $Q \approx 2 \times 10^7$. The achievable SNR is in the 10^3 to 10^4 range, limited by atomic detection shot noise; it is determined by the intensity of the detected beam, which in turn is limited by the effusive beam intensity and by unavoidable velocity filtering and hyperfine Zeeman state selection performed by the selector magnet. Among all the types of compact atomic clocks currently used in GNSS, the CFS is the closest one to the ideal of interrogating an isolated atom free of environmental perturbations. Even so, CFSs typically shift from white to flicker frequency noise behavior for long enough averaging times. Fluctuations in the DC magnetic field inside the resonant Ramsey cavity, or fluctuating phase or power asymmetries between the two branches of the Ramsey cavity are some of the dominant drivers of flicker frequency noise in these clocks (Bauch 2003).

The CFS on GPS SVN62 displays pure white noise behavior well beyond 10^5 s averaging time, with $\sigma_y(\tau) \approx 1.6 \times 10^{-11}/\sqrt{\tau}$ estimated from data published by Vannicola et al. (2010), and yielding a 5.4×10^{-14} 24-h frequency stability. The CFS on GLONASS R17 (Cernigliaro et al. 2013) flickers at $\sigma_y(\tau) \approx 3 \times 10^{-14}$ after averaging for about 16 h; we estimate its white frequency noise behavior to be $\sigma_y(\tau) \approx 5.5 \times 10^{-12}/\sqrt{\tau}$.

Rubidium atomic clock

A Rb atomic clock, or rubidium frequency standard (RFS) performs an optical/microwave double resonance experiment in a ^{87}Rb vapor cell enclosed in a microwave cavity (Camparo 2007). As shown in Fig. 4, resonance light from a ^{87}Rb discharge lamp is filtered by a ^{85}Rb vapor cell, shaping its spectrum so that the light can optically pump

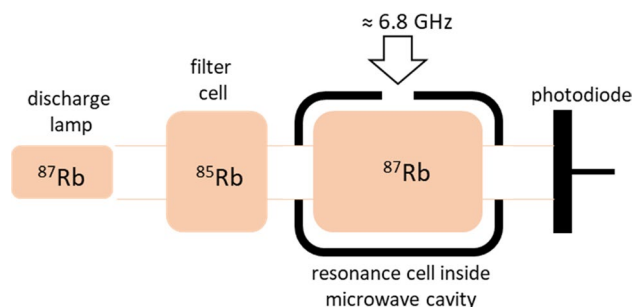


Fig. 4 Schematic diagram of a RFS physics package displaying its main elements: ^{87}Rb discharge lamp, ^{85}Rb filter cell, ^{87}Rb resonance cell inside a microwave cavity, and photodiode. Not shown are the lamp and cell ovens, magnetic shields and C-field coil

^{87}Rb atoms in the resonance cell, creating a population imbalance between the two hyperfine sublevels (Kastler 1957). In the absence of a near-resonant microwave field inside the cavity, the optical pumping light is transmitted through the vapor with relatively little absorption and detected by a photodiode. The presence of near-resonant microwaves in the cavity will equalize the population of the Rb hyperfine states, increasing light absorption in the vapor and decreasing the light detected by the photodiode. When the injected microwave frequency equals the hyperfine transition frequency, $\nu_0 \approx 6.8$ GHz, the photodiode signal will reach a minimum, providing the means to lock the microwave frequency to ν_0 .

The interrogation technique described above can provide very high signal-to-noise ratios of the order of 10^4 . The Doppler width of the microwave resonance signal is narrowed by adding a buffer gas into the resonant cell (Dicke 1953), resulting in a hyperfine transition line $Q \approx 10^7$, with the potential of yielding high white frequency noise stabilities. However, the interrogated atoms are exposed to strong environmental perturbations: fluctuations in the intensity and spectrum of the optical pumping light, collisions with the buffer gas molecules, etc. Unless great care is taken with all aspects of the design of the physics package, an RFS will transition to the random walk frequency noise regime for relatively short averaging times, of the order of 10^3 – 10^4 s.

RAFS25, a GPS IIF RFS undergoing life test at the US Naval Research Laboratory (NRL), displays pure white frequency noise behavior well beyond 24-h averaging time. We estimate from data published by Vannicola et al. (2010) $\sigma_y(\tau) \approx 1 \times 10^{-12}/\sqrt{\tau}$ yielding a 3×10^{-15} 24-h frequency stability. The Galileo R-RAFS prototype (Droz et al. 2015) displays white frequency behavior, with $\sigma_y(\tau) \approx 2 \times 10^{-12}/\sqrt{\tau}$, transitioning toward random walk frequency noise after averaging for about 17 h, and yielding a 10^{-14} 24-h frequency stability. A prototype RFS for BeiDou developed at the Wuhan Institute of Physics and Mathematics (Mei et al 2016) displays pure white frequency noise behavior beyond 10^5 s, with $\sigma_y(\tau) \approx 7 \times 10^{-13}/\sqrt{\tau}$ and a 3×10^{-15} 24-h frequency stability. The output frequency of a RFS will typically display significant slow drift, which can usually be well approximated by a linear function of time, $(\nu - \nu_0)/\nu_0 \approx \beta t$. If left uncorrected, after a time interval T the frequency drift will result in an accumulated time error $\Delta T \approx \beta T^2/2$. The GNSS ground control estimates and updates the frequency drift rate β of the satellite clocks, and the drift rates are included in the navigation message, allowing the user's receiver to correct for that error. RFS drift rates can be as low as a few parts in 10^{14} /day (Vannicola et al. 2010).

Passive hydrogen maser

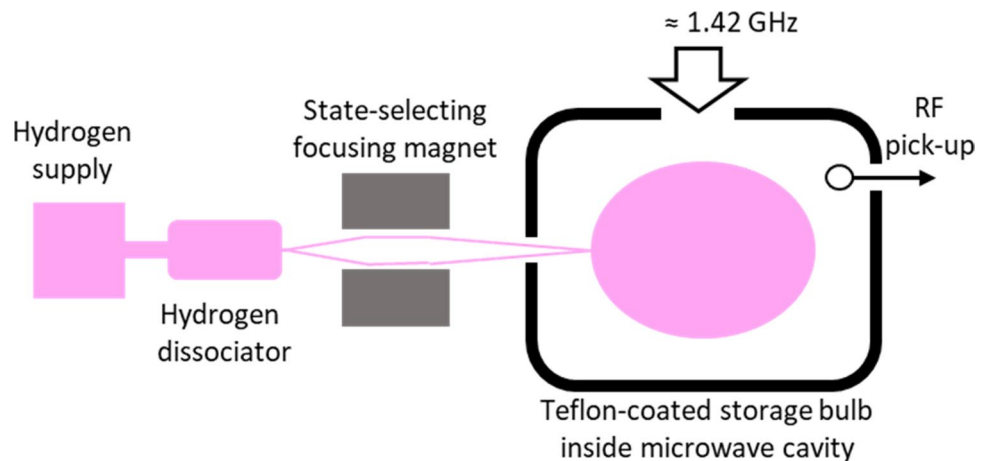
As hinted by its name, a hydrogen maser performs microwave amplification by stimulated emission of radiation. The fundamentals (and most of the technical details) of the design and operation of a hydrogen maser are discussed by Kleppner et al. (1965). As shown in Fig. 5, a hydrogen reservoir feeds molecular hydrogen into a rf-discharge dissociator that outputs a beam of atomic hydrogen. A quadrupole or hexapole magnet focuses the atoms in the higher-energy hyperfine state at the entrance orifice of a Teflon-coated glass storage bulb; the atoms in the lower-energy hyperfine state diverge out of the bulb entrance. The Teflon coating

allows H atoms to collide with the walls without changing their hyperfine state; in that way, a gas of H atoms in the upper hyperfine state fills the bulb. In the original Kleppner experiment, a very high Q cavity tuned to the $\nu_0 \approx 1.42$ GHz hyperfine transition frequency in hydrogen provided enough gain for the maser to act as an oscillator; a microwave pickup antenna coupled the 1.42 GHz signal to the output of the device. Active hydrogen masers, used as time and frequency standards in many laboratories, operate in this manner but are not practical space clock candidates because of their size: A relatively large microwave cavity is mandated by the 21 cm wavelength of the hydrogen hyperfine transition. Different approaches have been explored to reduce the cavity size. The preferred one for GNSS satellite clocks is the passive hydrogen maser (PHM), where the physics package acts as an extremely high Q tuned amplifier. When the frequency of the injected microwaves equals the hyperfine transition frequency $\nu_0 \approx 1.42$ GHz, the output of the PHM physics package reaches a maximum, providing the means to lock the microwave frequency to ν_0 . Other approaches involve dielectric loading of the microwave cavity or adding high, narrow-band external gain.

The PHM can provide high hyperfine transition line Q values, $Q \approx 5 \times 10^8$, yielding very good white frequency noise performances with SNR of the order of 10^4 . However, the H atoms in the storage bulb are exposed to strong environmental perturbations, particularly collisions with the bulb wall, causing the transition frequency “wall shift,” and the interaction with the interrogating microwaves, causing the transition frequency “cavity pulling” shift. In PHM, the colored frequency noise introduced by those perturbations becomes dominant for averaging times of the order of 10^4 s.

The Galileo PHM (Droz et al. 2008) displays white frequency noise behavior $\sigma_y(\tau) \approx 6 \times 10^{-13}/\sqrt{\tau}$, flickering at 7×10^{-15} after averaging for about an hour, and yielding a 7×10^{-15} 24-h frequency stability. The BeiDou PHM (Li et al. 2016) displays white frequency noise behavior $\sigma_y(\tau) \approx$

Fig. 5 Schematic diagram of a PHM physics package displaying its main elements: H₂ source, H₂ dissociator, state-selecting focusing magnet, microwave cavity, Teflon-coated H storage bulb and microwave pickup antenna. Not shown are the magnetic shields, the C-field coil and the ion pump and hydrogen getters required to keep the physics package under vacuum



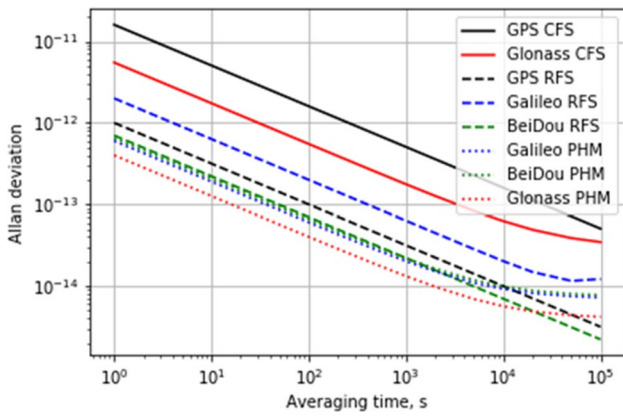


Fig. 6 Representative Allan deviation versus averaging time for a variety of GNSS flight clocks

Table 1 Typical SWaP parameters and SIS-URE contributions (δR_C) 24 h after clock update for current GNSS clock technologies

	Volume (l)	Mass (kg)	Power (W)	δR_C @ 24 h (m)
CFS	14	13	30	3.50
RFS	5	7	30	0.19
PHM	40	25	55	0.45

$6 \times 10^{-13}/\sqrt{\tau}$ flickering at 7×10^{-15} after averaging for about 3 h, and yielding a 7×10^{-15} 24-h frequency stability. In the Russian Federation, Vremya-CH has developed a PHM for use in GLONASS (Belyaev et al. 2013) displaying white frequency noise behavior $\sigma_y(\tau) \approx 4 \times 10^{-13}/\sqrt{\tau}$ flickering at 4×10^{-15} after averaging for about 6 h, and yielding a 4×10^{-15} 24-h frequency stability.

2020 GNSS atomic clocks: the systems engineer’s view

Figure 6 shows representative Allan deviation curves for all the GNSS clock technologies discussed above. Solid, dashed or dotted lines indicate CFS, RFS or PHM technologies, respectively, and the color of the curve indicates the specific GNSS system: black for GPS, red for GLONASS, blue for Galileo and green for BeiDou. As noted above, the Vremya-CH GLONASS candidate PHM has not flown yet. Additionally, Spectratime is developing a miniaturized PHM for Galileo (Rochat 2016) displaying a frequency stability essentially identical to that of the GPS RAFS for averaging times up to 3×10^4 s. (Data for longer averaging times are not available.)

Table 1 lists typical volumes, weights and power requirements for the three clock technologies in discussion: CFS, RFS and PHM. Their typical contributions to

SIS-URE 24 h after clock update are also listed. The Galileo RFS and PHM are significantly smaller and lighter.

The two dominant contributions to a GNSS SIS-URE are δR_E , due to the uncertainties in the satellite ephemeris, and δR_C , caused by the onboard time uncertainty (Heng et al. 2012). Currently, the clock contributions are either larger than or similar to the ephemeris contributions (Montenbruck et al. 2020). Thus, improving the onboard clock timekeeping ability will have a direct bearing on the reduction in a GNSS SIS-URE. In what follows, we will focus exclusively on δR_C , the direct contribution of the frequency noise of the satellite clock to SIS-URE.

In general, the clock contribution to SIS-URE after an update interval τ_{up} has elapsed will be given by $\delta R_C = c\delta\tau_{up}$, where c is the speed of light and $\delta\tau_{up}$ is the accumulated clock time uncertainty just before the next update from the ground. The maximum clock time error expected over the τ_{up} interval will be (Riley 2008)

$$\max(\delta\tau_{up}) = k_\beta \cdot \sqrt{2} \cdot \sigma_y(\tau_{up}) \cdot \tau_{up} \tag{2}$$

where k_β depends on the desired confidence level β . For $\beta=95\%$, $k_\beta=1.77$.

For a system with a concept of operations involving 24-h clock updates, the RFS technology is clearly the current optimal choice; it combines the best SWaP parameters and the smallest contribution to the 24-h SIS-URE. CFS technology is not competitive. The Vremya-CH PHM performs competitively, but at the cost of a very high SWaP penalty.

Dropping the satellite clock out of the navigation error budget

Discarding all sources of ranging error except for the clock and ephemeris, and assuming that δR_C and δR_E are uncorrelated, the range error $\delta R \approx [\delta R_E^2 + \delta R_C^2]^{1/2} = [1 + \kappa^2]^{1/2} \delta R_E$, where $\kappa = \delta R_C / \delta R_E$. Taking $\kappa < 1$ for the sake of argument, to first order in κ^2 we can write $\delta R \approx [1 + \kappa^2/2] \delta R_E$. If $\kappa \leq 0.3$, then the clock error contribution to the total ranging error will be less than 5%. In what follows, we will not consider possible contributions to the clock error caused by estimation errors in the navigation message clock parameters, and we will attribute the full clock error to its frequency noise, as measured by its Allan deviation.

If the satellite clock frequency stability for $\tau \leq \tau_{up}$ stays in the white frequency noise regime, $\sigma_y(\tau) = A/\tau^{1/2}$, then by (2) the maximum accumulated time error between updates will be, to a 95% confidence level, $\max(\delta\tau_{up}) \approx 2.5A\sqrt{\tau_{up}}$. Consequently, $\delta R_C = c\delta\tau_{up} \approx \kappa\delta R_E$ requires

$$A \approx \frac{\kappa \cdot \delta R_E}{(7.5 \times 10^8 \text{ m/s}) \tau_{\text{up}}^{1/2}} \tag{3}$$

A GNSS satellite clock that increases the SIS-URE by less than 5% above the ephemeris uncertainty alone will effectively drop the onboard time error out of the navigation error budget, and as the above shows, this can be achieved if $\kappa \leq 0.3$. Assuming that the clock frequency stability for $\tau \leq \tau_{\text{up}}$ stays in the white frequency noise regime, that condition will be satisfied if $A\sqrt{\tau_{\text{up}}} \leq \delta R_E / (2.5 \times 10^9 \text{ m/s})$. This in turn can be achieved either by reducing τ_{up} by system design and concept of operations, or by investing in clock development to reduce A. Although the trade-off is clearly a matter of systems engineering judgment, in what follows, we focus on the latter approach.

Given the assumptions noted above, $\sigma_y(\tau) = A/\tau^{1/2}$ for $\tau \leq \tau_{\text{up}}$ and $\kappa = 0.3$, Fig. 7 shows the required values of A to drop the clock out of the SIS-URE budget as a function of update interval for $\delta R_e = 0.1, 0.2$ and 0.5 m. Representative values of current ephemeris errors for GPS, GLO-NASS, Galileo and BeiDou are 0.23, 0.48, 0.14 and 0.12 m, respectively (Montenbruck et al. 2020). The conclusion to be drawn from Fig. 7 is that for ephemeris uncertainties of the order of tens of centimeters and update intervals of many hours, spacecraft clocks will require white frequency noise-limited stabilities in the low parts in $10^{-13}/\sqrt{\tau}$ if the clock is no longer to contribute significantly to the SIS-URE.

GNSS clock desideratum

As noted by Montenbruck (2020), the current ephemeris error in GPS is of the order of 0.2 m; 5% of that amounts to about 0.01 m. Even assuming that the ephemeris errors

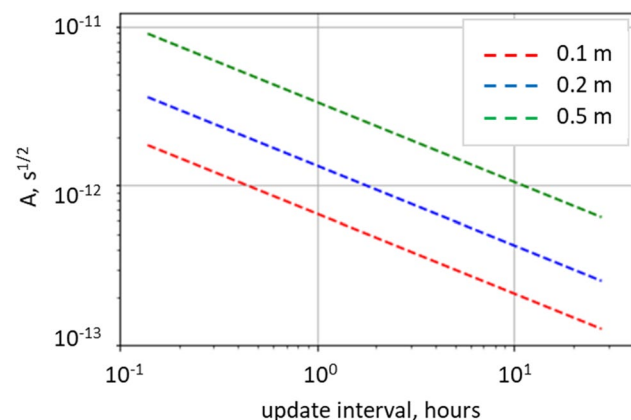


Fig. 7 Allan deviation white frequency noise coefficient to keep the increase in SIS-URE due to the clock below 5% of the ephemeris contribution, for ephemeris errors of 0.1, 0.2 and 0.5 m

are significantly lower than 0.2 m, it is difficult to imagine real-time positioning or navigation applications that would require better than 1 cm SIS-URE, so we will set the desideratum for the clock contribution to SIS-URE 24 h after the last update at that level, requiring a white frequency noise Allan deviation $\sigma_y(\tau) \approx 2.7 \times 10^{-13}/\sqrt{\tau}$, three to four times better than the current GPS RAFS.

In our opinion, that sets the ultimate technology goal for GNSS satellite clocks: a clock that operates in the white frequency noise regime for 10^5 s or longer, with an Allan deviation $\sigma_y(\tau) \approx 3 \times 10^{-13}/\sqrt{\tau}$. Striving for better performance than that is overkill: It buys nothing in terms of GNSS navigational capabilities. Operation in the white frequency noise regime implies that the clock frequency noise is dominated by its fundamental physics, not by sensitivity to fluctuations in the environment of the interrogated atoms. That should result in more predictable performances of production clocks, with less significant clock-to-clock performance variation. It should also result in smaller clock environmental sensitivities and smaller linear frequency drift coefficients. Using the 24-h update interval as our baseline requirement provides for stand-alone satellite robustness, even if the system concept of operations allows for more frequent updates.

Other important considerations for a GNSS satellite clock are operating life, reliability, SWaP and cost. Of those, the cost of the clocks has the least impact, since the cost of any reasonably sized set of clocks in the GNSS satellite navigation payload is typically a small fraction of the total mission cost, including launch, while the clock ultimately determines the performance of the navigation payload.

Generally, the expected GNSS satellite operating life ranges from 10 to 15 years. The expected operating life of a GNSS atomic clock should be such that a set of a few clocks will support the expected mission duration with very high reliability. A critical element in assessing clock operating life is its use of consumables, but the determination of what is a consumable can be non-trivial. It is easy to see that the cesium load in a CFS oven or the hydrogen load in a PHM reservoir is a consumable. After some thought, it becomes evident that the cesium or hydrogen gettering capacities for those clock technologies are also “consumables.” But when looking at the RFS technology, where everything takes place within vacuum-tight glass envelopes, it is easy to assume that there are no consumables. However, RFS exhibited early failures because of discharge lamp Rb loss (Volk et al. 1984), and, much later, because of discharge lamp Xe buffer gas loss (Jaduszliwer et al. 2015). The lesson here is that confidence in the operating life expectation of a clock requires a thorough understanding of all possible failure modes. As the old saying goes, “what you don’t know that you don’t know is what will kill you.” Thus, life testing should be part of the development of any new GNSS clock

technology, and it should be started as early as possible in the development process.

As for SWaP, systems engineers should avoid placing arbitrary a priori hard constraints on those parameters. The need to save volume, weight and power is clear, but the push to save that last 10% in any of those parameters may compromise clock performance or reliability in unpredictable ways. Experience suggests that it should be possible to design a clock that will meet the desired performance parameters while staying within an approximately 10 l, 10 kg and 40 W SWaP box; actual hard bounds on those parameters should be placed after the challenges presented by a specific clock technology are well understood, and not before.

What clocks are there in the future of GNSS?

Several competing clock technologies are now being offered for use in future GNSS satellites. In particular, we have discussed why, as far as navigation is concerned, white frequency noise performance much better than $\sigma_y(\tau) \approx 3 \times 10^{-13}/\sqrt{\tau}$ out to 10^5 s averaging time should not be a deciding factor in adopting one technology over another. Instead, all technologies offering performance at least as good as that level should be considered as equally well suited for onboard GNSS timekeeping, and choices among those technologies should be made on the basis of technology maturity, SWaP, operational life and clock reliability.

Mercury ion clock

The Hg^+ clock or mercury frequency standard (MFS), also known in different configurations as the Linear Ion Trap Standard (LITS), Mercury Atomic Frequency Standard (MAFS) and Deep Space Atomic Clock (DSAC), was originally developed by researchers at Hewlett Packard Corporation (Cutler 1983), but truly matured by scientists at NASA's Jet Propulsion Laboratory (JPL). Its reference frequency is the $\nu_0 \approx 40.5$ GHz hyperfine transition in the ground state of the $^{199}\text{Hg}^+$ ion. Since the ions carry an electrical charge, they can be confined by electromagnetic fields. The early trapped mercury ion clock using a three-dimensional RF Paul ion trap was not very successful because space charge limited the number of ions that could be confined in the quasi-spherical symmetry ion cloud, resulting in poor SNR. That problem was resolved at JPL by replacing the three-dimensional RF trap by a linear RF trap consisting of a Paul quadrupole RF mass filter capped at both ends by electrodes at a high enough positive potential (Paul et al. 1958); the cylindrical symmetry of this arrangement allows for trapping a large number of ions by reducing space charge effects. While all the atomic clock technologies currently used in GNSS allow for continuous microwave interrogation of the

atomic frequency reference, in the MFS interrogation takes place as a sequence of discrete three-step events: atomic state preparation, atom–microwave interaction and atomic state analysis/detection (Prestage et al. 1989). The physics package of the MFS is shown schematically in Fig. 8.

In the first step, an electron gun placed at one of the ends of the trap is turned on for a short time to provide a large enough number of $^{199}\text{Hg}^+$ ions. The ions thermalized by collisions with buffer gas (He or Ne) atoms are trapped by the quadrupole RF field and are then optically pumped by the light from a ^{202}Hg discharge lamp to provide the necessary population imbalance between the two hyperfine sublevels of the trapped ions. In the second step, the lamp is turned off, or its light is blocked, and the $^{199}\text{Hg}^+$ ions interact for an interrogation time T with $\nu \approx 40.5$ GHz radiation injected into the trap by a microwave horn. In the third step, the discharge lamp light illuminates again the $^{199}\text{Hg}^+$ ions. In the absence of a near-resonant microwave field, the $^{199}\text{Hg}^+$ ions will remain in the hyperfine level populated by optical pumping and will not absorb light from the lamp. The presence of near-resonant microwaves will repopulate the depleted $^{199}\text{Hg}^+$ hyperfine level, and the ions will absorb light from the lamp and fluoresce; the photomultiplier will then detect some of that fluorescent light. When the injected microwave frequency equals the hyperfine transition frequency, $\nu = \nu_0$, the photomultiplier signal will reach a maximum, providing the means to lock the microwave frequency to ν_0 . To maximize the signal, the microwave power level is adjusted to provide a full “Rabi flop” (Ramsey 1956) during the interrogation time T . The microwave linewidth can be reduced by increasing T , and very small linewidths can be achieved. It is important to stress that because of the significant dead

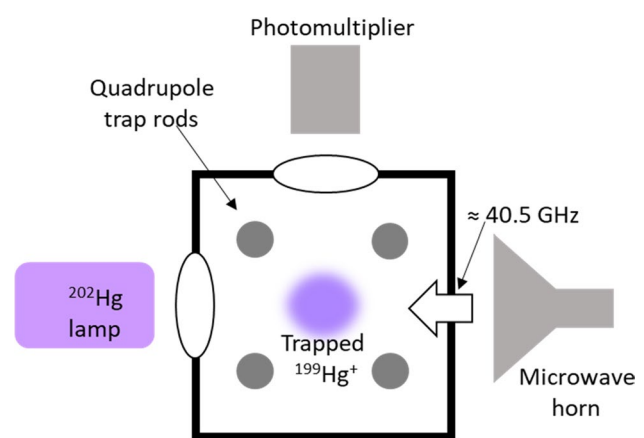


Fig. 8 Schematic cross-sectional diagram of an MFS physics package displaying its main elements: ^{202}Hg discharge lamp, RF quadrupole linear trap, trapped $^{199}\text{Hg}^+$ columnar cloud, microwave horn and photomultiplier. Not shown are the trap end caps, the electron gun, ^{199}Hg source and getter pump. The vacuum envelope contains a buffer gas (helium or neon) at a very low pressure and ^{199}Hg vapor

time associated with the three-step pulsed interrogation, the MFS technology requires a highly stable local oscillator.

Because of its high ν_0 and very small $\Delta\nu$, the MFS has an extremely high hyperfine transition line Q , and so can provide very high-frequency stabilities. While MFS technology would indeed be novel as a GNSS clock technology, MFS have been built and operated for over 25 years; they are well understood, and the MFS technology maturity offers a sound basis for risk mitigation if the MFS was to be considered as the GNSS desideratum clock. Between 1997 and today, JPL has delivered multiple MFS to NASA's Deep Space Network (DSN) and the US Naval Observatory under the LITS (Linear Ion Trap Standard) label.

Recognizing its potential as a space clock technology, scientists at JPL started in 2003 to develop smaller MFS prototypes having reasonable SWaP parameters and capable of operating with a high-quality OCXO as the local oscillator. A breadboard device (Tjoelker et al. 2011) was developed for possible use in GPS; it consumed 40 W, and once fully engineered, it was expected to have a few liters volume and a few kilograms mass. Having a hyperfine transition line $Q \approx 8 \times 10^{10}$, it operated in the white noise frequency regime for $10 \text{ s} < \tau \leq 10^5 \text{ s}$ with an Allan deviation $\sigma_y(\tau) \approx 1.5 \times 10^{-13}/\sqrt{\tau}$; for $\tau < 10 \text{ s}$ $\sigma_y(\tau) \approx 10^{-13}$, determined by the local oscillator. The Deep Space Atomic Clock (DSAC) was developed (Tjoelker et al. 2016) to demonstrate the value of high stability atomic clocks for deep space navigation and radio science. The NASA Technology Demonstration DSAC mission was launched into Earth orbit on June 25, 2019; it has been operating successfully, and NASA has extended the mission duration for another year (Cofield 2020).

A prototype MFS for space applications under development at the Key Laboratory of Atomic Frequency Standards of the Chinese Academy of Sciences (Liu et al. 2020) has demonstrated a white frequency noise Allan deviation $\sigma_y(\tau) \approx 4.5 \times 10^{-13}/\sqrt{\tau}$ for $t \leq 4 \times 10^4 \text{ s}$, with no indication of the presence of colored frequency noise up to that averaging time. Its SWaP parameters are 16.4 l, 15.12 kg and 66 W.

Pulsed optically pumped rubidium atomic clock

The pulsed optically pumped rubidium atomic clock (or pulsed optically pumped rubidium frequency standard, POP-RFS) looks very similar to the RFS, except that it uses a laser as the optical pumping light source, rather than a discharge lamp, and it operates in a pulsed, instead of continuous, interrogation fashion (Levi et al. 2013).

The physics package of a POP-RFS is shown schematically in Fig. 9. As in the MFS, interrogation takes place as a sequence of discrete three-step events: atomic state preparation, atom–microwave interaction and atomic state analysis/detection. In the first step, a semiconductor laser operating at 780 nm optically pumps the hyperfine sublevels of

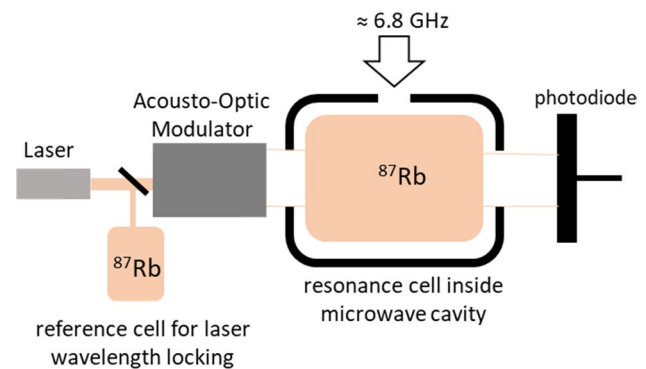


Fig. 9 Schematic diagram of a POP-RFS physics package displaying its main elements: 780 nm laser, wavelength reference cell, acousto-optic modulator, resonance cell containing ^{87}Rb vapor and enclosed in a microwave cavity, and photodiode. Cell ovens, magnetic shields and C-field coil are not shown

the ^{87}Rb atoms in the resonance cell. A second ^{87}Rb vapor cell provides an optical wavelength reference to lock the laser output wavelength. In the second step, the acousto-optic modulator blocks the laser light, and the Rb atoms interact with $\nu \approx 6.8 \text{ GHz}$ microwave pulses timed using a scheme known as Ramsey interrogation (Ramsey 1956). In the third step, the laser light illuminates again the ^{87}Rb atoms. In the absence of a near-resonant microwave field, the ^{87}Rb atoms will remain in the hyperfine level populated by optical pumping and will not absorb light from the laser. The presence of near-resonant microwaves will repopulate the depleted ^{87}Rb hyperfine level, and the atoms will absorb light from the laser. When the injected microwave frequency equals the hyperfine transition frequency, $\nu = \nu_0$, the photodiode signal will reach a minimum, providing the means to lock the microwave frequency to ν_0 . Again, because of the dead time associated with the three-step pulsed interrogation, the POP-RAFS technology imposes somewhat stronger requirements on the frequency stability of the local oscillator, compared with the lamp-pumped RAFS. However, a major advantage of the three-step pulsed interrogation is that the atoms interact with the microwaves in the absence of perturbing laser light. Recent research suggests that jumps in lamplight for the lamp-pumped RAFS are a major contributor to the clock's observed random walk frequency noise (Formichella et al. 2017); the POP-RAFS would therefore have no such issue.

The Ramsey interrogation technique results in a narrower hyperfine transition linewidth than in the case for the lamp-pumped RFS, yielding a hyperfine transition line $Q \approx 4.5 \times 10^7$. The prototype POP-RFS at the Istituto Nazionale di Ricerca Metrologica (INRiM) displayed a white frequency noise Allan deviation $\sigma_y(\tau) \approx 1.7 \times 10^{-13}/\sqrt{\tau}$ for $\tau < 10^4 \text{ s}$ (Levi et al. 2013). Shen et al. (2020) reported a white frequency noise Allan deviation for a POP-RFS at the Shanghai

Institute of Optics and Fine Mechanics (SIOM) of $\sigma_y(\tau) \approx 2.8 \times 10^{-13}/\sqrt{\tau}$ for $\tau < 10^4$ s. In their prototype design, Levi et al. (2013) observed that colored noise became significant for averaging times longer than an hour, which was attributed to a higher-than-expected sensitivity to temperature fluctuations in their physics package design. A POP-RFS engineered for space operation is now under development by a Leonardo SpA/INRiM collaboration (Arpesi et al. 2018), with an expected SWaP of 17 l, 9 kg and 50 W.

Optical rubidium atomic clock

A completely different architecture for a novel space clock was developed at the US Air Force Research Laboratories (AFRL) and is described by Phelps et al. (2018). Instead of locking the frequency of a RF OCXO to an atomic hyperfine transition in the microwave frequency range, the optical rubidium frequency standard (O-RFS) locks the frequency of a near-infrared laser to an atomic optical transition, using quasi-resonant Doppler-free two-photon spectroscopy in a Rb vapor cell. The concept (Millerioux et al. 1994) exploits the fact that it is possible to excite the $5S_{1/2} \rightarrow 5D_{5/2}$ optical transition in ^{85}Rb by absorbing two 778 nm photons; if the two photons are counterpropagating, the excitation will be unaffected by the Doppler effect. The optical transition has a line $Q \approx 10^9$. On its way back to the ground state, the excited ^{85}Rb atom will emit a 420 nm photon that can be detected very efficiently by a photomultiplier; the background of 778 nm light can be easily filtered out, leading to excellent detection SNR.

A block diagram of the O-RFS physics package is shown in Fig. 10. Phelps et al. (2018) used an AlGaAs diode laser as their 778 nm IR light source; as an alternative, a frequency-doubled 1556 nm telecom fiber laser was used by Lemke et al. (2017). The retroreflector at the back of

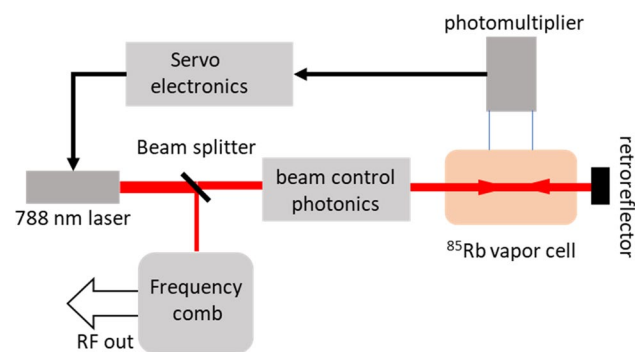


Fig. 10 Block diagram of an O-RFS, displaying its main components: 778 nm IR laser, beam control photonics, ^{85}Rb vapor cell, beam retroreflector and photomultiplier. The beam splitter directs a fraction of the light output of the laser into a frequency comb generator. Not shown are the cell oven, magnetic shields and a blue filter preventing IR light from scattering into the photomultiplier

the ^{85}Rb vapor cell provides the counterpropagating beam required for Doppler-free two-photon spectroscopy. The blue (420 nm) fluorescence emitted as ^{85}Rb atoms excited to the $5D_{5/2}$ state decay back to their ground state is detected by the photomultiplier; when the laser is tuned at the atomic $5S_{1/2} \rightarrow 5D_{5/2}$ transition frequency, $\nu = \nu_0$, the photomultiplier signal will reach a maximum, providing the means to lock the laser frequency to ν_0 . Figure 10 looks deceptively simple; the box labeled “beam control photonics” stands for several fairly complex photonics/electronics control loops.

The optical frequency reference provided by the O-RFS is in the optical domain, $\nu_0 \approx 3.85 \times 10^{14}$ Hz. For practical O-RFS applications, that frequency must be translated to the RF domain without losing frequency stability. This can be accomplished by using the frequency comb technique described by Diddams et al. (2000). A beam splitter feeds a small fraction of the laser light to produce an optical beat note with a compact fiber frequency comb generator similar to the one described by Sinclair et al. (2015). The Phelps et al. (2018) O-RFS realization showed a white frequency noise Allan deviation $\sigma_y(\tau) \approx 5 \times 10^{-13}/\sqrt{\tau}$ for integration times shorter than 200 s, with random walk frequency noise becoming dominant for longer averaging times. Their estimated SWaP parameters for the optical portion of the O-RFS are approximately 30 l, 8.4 kg and 80 W. The main contributors to colored frequency noise are laser power fluctuations and Rb vapor density fluctuations caused by a fluctuating oven temperature. The Lemke et al. (2017) O-RFS realization showed a white frequency noise Allan deviation $\sigma_y(\tau) \approx 5 \times 10^{-13}/\sqrt{\tau}$ for averaging times shorter than an hour, with colored noise becoming dominant for longer integration times. That realization used a frequency-doubled telecom laser, likely leading to a larger, heavier clock requiring higher power.

Concluding thoughts

Among the technologies described in the preceding section, the MFS probably presents the least technical risk. It has already demonstrated that it meets the performance desideratum in a flight design; the dominant sources of colored frequency noise are understood and well under control, and it can be engineered to meet the previously discussed SWaP goals. It has a quarter of a century of operational history as a ground frequency standard, and its failure modes are understood. As is the case with the RFS, the most likely source of surprises will be its rf-discharge lamp, implying that for this technology, lamp reliability and lamp operational life must be given close attention.

The POP-RFS short-time performance meets the $\sigma_y(\tau) \approx 3 \times 10^{-13}/\sqrt{\tau}$ desideratum. The O-RFS demonstrated performance falls slightly short, but it is likely that it can be

improved enough to meet it. In both cases, colored frequency noise becomes dominant for averaging times longer than an hour, though in each case the source of that noise appears to be known: for the POP-RFS, temperature gradient noise, which can be mitigated via careful attention to design; and in the case of the O-RFS, AC-Stark shift fluctuations, which can be mitigated via careful attention to laser intensity stability. Nevertheless, for these two technologies, additional work will be needed to understand their sources of colored frequency noise better and to develop SWaP-efficient means of mitigation.

Both the POP-RFS and O-RFS technologies make use of lasers and other photonic components. Much of the photonic components and devices available for use in new clock technologies were developed for the wideband communications industry. The devices used in the infrastructure of that industry typically have high reliability ratings. But they were not developed for use in space, and their suitability for use in satellites cannot be taken for granted. Besides the obvious need for radiation hardness testing, their reliability, operating life and performance in a vacuum and in the thermal spacecraft environment must be assessed, as well as their ability to survive the launch shock and vibration environment. Mode-hops, which are common in many types of semiconductor lasers, will cause the clock to lose frequency lock and thus must be avoided; a GNSS clock laser should be able to operate without mode-hops for many years. In our opinion, the O-RFS presents a higher technical risk than the POP-RFS because of its extensive use of photonic components, the added complexity presented by the need to use a femtosecond laser frequency comb to translate frequencies from the optical to the RF domain, and the large SWaP parameters of current prototypes.

Other clock technologies have been proposed as candidate advanced atomic clocks for GNSS. The frequency stability of cesium atomic beam clocks is limited by a relatively poor SNR. In the classical CFS clock that uses constant field gradient magnets for hyperfine state selection and analysis, a very small fraction of the atoms effusing from the cesium oven ends up at the detector. Replacing magnetic state selection by optical pumping with a diode laser, and hot wire ionizer detection by optical fluorescence detection can improve the SNR by orders of magnitude. Optically pumped, optically detected cesium beam clocks for GNSS applications have been demonstrated by Lutwak et al. (2001), achieving in their high-performance configuration a white frequency noise Allan deviation $\sigma_y(\tau) \approx 1.5 \times 10^{-12}/\sqrt{\tau}$ for averaging times up to a day (with no signs of flickering), and by Schmeissner et al. (2017), who reported a white frequency noise Allan deviation $\sigma_y(\tau) \approx 2 \times 10^{-12}/\sqrt{\tau}$ for $\tau \leq 10^4$ s, flickering for longer integration times. That performance would make them competitive with the best GNSS RFS, although at the cost of a significant SWaP penalty. However,

there is no clear path for that technology to achieve the performance expected for the desideratum clock.

The development of laser cooling and trapping of neutral alkali atoms during the 1980s precipitated a revolution in time metrology. Laser-cooled atoms can have speeds as low as a few cm/s, allowing for much longer microwave interrogation times, and thus resulting in very high hyperfine line. Kasevich et al. (1989) demonstrated the feasibility of a Zacharias-type fountain clock, and over the next decade fountain clocks became the primary time and frequency standard in metrology laboratories around the world. Fountain clocks require gravity for their operation, but before the 1990s were over, cold atom clocks for space applications were under consideration in Europe and the USA.

Lemondé et al. (1997) described a cold cesium atom clock capable of operating in microgravity. It was developed by the French Centre National D'Etudes Spatiales (CNES) for eventual deployment in the International Space Station (ISS) for scientific and metrology applications. A cold rubidium atom space clock of similar architecture was developed for the Chinese Manned Space Program (Liu et al. 2018) and deployed on board the Chinese Space Laboratory Tiangong-2. Those clocks are significantly smaller and lighter than metrology-class atomic fountains, but are still too large, heavy and power-hungry for GNSS onboard clock applications.

Compact cold atom clocks for space applications were proposed by Buell and Jaduszliwer (1999) and Heavner et al. (2011). The Allan deviations achieved by those clocks could easily meet $\sigma_y(\tau) \approx 3 \times 10^{-13}/\sqrt{\tau}$ for $\tau \leq 10^5$ s and could have SWaP parameters falling within the 10 l, 10 kg and 40 W box. However, slow atom trajectories in the satellite microgravity environment will be very different from those in the terrestrial test bench. The “test as you fly” systems engineering paradigm requires each individual GNSS clock to be tested on the ground operating in the same way as it would in space. A cold atom clock could be designed for dual operation on the ground and in microgravity, and the technology could be validated in a low-cost experimental satellite, but it still would not be able to meet the “test as you fly” requirement, making the cold atom clock technology less desirable for GNSS onboard clocks.

In conclusion, there are three clock technologies under current development that could meet the requirements for the ultimate GNSS onboard clock: the MFS, the POP-RFS and the O-RFS. Of those, and strictly from a technology perspective, the MFS is the one closest to be ready for the actual design of a GNSS flight clock. The other two need varying levels of additional effort, as well as additional work to assess the reliability and operational lifetimes of the photonic components and devices used in their physics packages. The O-RFS also needs to demonstrate the ability of a prototype to fall within the desired SWaP parameters

box of 10 l, 10 kg and 40 W. This is not to say that the MFS does not have its own issues to address for GNSS applications (Camparo and Driskell, 2015), it only means that of the three technologies, the MFS is furthest along for future GNSS operation.

References

- Allan DW, Weiss MA, Pepler TK (1989) In search of the best clock. *IEEE Trans Instrum Meas* 38:624–630
- Arpesi P et al (2018) Development status of the Rb POP space clock for GNSS applications. In: Proceedings of the 2018 European frequency and time forum, IEEE Press, Piscataway, NJ, USA, pp 72–74
- Bauch A (2003) Cesium atomic clocks: functions, performance and applications. *Meas Sci Technol* 14:1159–1173
- Beard RL, Murray J, White JD (1986) GPS Clock Technology and the Navy PTTI Program at the US Naval Research Laboratory. In: Proceedings of the 18th annual precise time and time interval (PTTI) applications and planning meeting, pp 37–53
- Belyaev A, Biriukov A, Demidov N, Likhacheva L, Medvedev S, Myasnikov A, Pavlenko Y, Sakharov B, Smirnov P, Storoyev E, Tulyakov A (2013) Russian hydrogen maser for space applications. In: Proceedings of the 2013 precise time and time interval systems and applications meeting, Institute of navigation, Nashville, TN, USA, pp 87–93
- Buell W, Jaduszliwer B (1999) Compact CW cold beam cesium atomic clock. In: Proceedings of the 1999 joint meeting of the European frequency and time forum and the IEEE international frequency control symposium, IEEE Press, Piscataway, NJ, USA, pp 85–87
- Camparo JC, Frueholz RP, Dubin AP (1997) Precise time synchronization of two milstar communications satellites without ground intervention. *Int J Satellite Commun* 15:135–139
- Camparo JC, Moss SC, LaLumondiere SD (2004) Space System Time-keeping in the Presence of Solar Flares. *IEEE Aerosp Electron Syst Mag* 19(5):3–8
- Camparo JC (2007) The Rubidium atomic clock and basic research, *Physics Today*, November 2007, pp 33–39, American Institute of Physics, Washington
- Camparo JC and Driskell TU (2015) The mercury-ion clock and the pulsed-laser rubidium clock: Near-term candidates for future GPS deployment, Aerospace Technical Report No. TOR-2015–03893
- Cernigliaro A, Vallorea S, Galleani L, Tavella P (2013) GNSS Space Clocks: Performance Analysis. In: Proceedings of the 2013 international conference on localization and GNSS, IEEE Press, Piscataway, NJ, USA, pp 1–5
- Cofield C (2020) NASA extends Deep Space Atomic Clock mission, Jet Propulsion Laboratory, California Institute of Technology, <https://www.jpl.nasa.gov/news/news.php?feature=7687> Accessed 25 June 2020
- Cutler, L.S., Giffard, R.P., McGuire, M.D. (1983) Mercury-199 trapped ion frequency standard: Recent theoretical progress and experimental results. In: Proceedings of the 37th annual symposium on frequency control, IEEE, Piscataway, NJ, USA, pp 32–36
- Dicke RH (1953) The effect of collisions upon the Doppler width of spectral lines. *Phys Rev* 89:472–473
- Diddams SA, Jones DJ, Ye J, Cundiff ST, Hall J, Ranka J, Windeler RS, Holzwarth R, Udem T, Hansch TW (2000) Direct link between microwave and optical frequencies with a 300 THz femtosecond laser comb. *Phys Rev Lett* 84:5102–5105
- Droz F et al (2008) Galileo rubidium standard and passive hydrogen maser. In: DelRe E, Ruggieri M (eds) *Satellite communications and navigation systems*. Springer, New York, pp 133–139
- Droz F, Rochat P, Boillat S., Scheidegger B (2015) GNSS RAFS latest improvements. In: Proceedings of the 2015 joint conference of the IEEE frequency control symposium and the European forum on frequency and time, IEEE Press, Piscataway, NJ, USA, pp 637–642
- Dupuis RT, Lynch TJ, Vaccaro JR (2008) Rubidium frequency standard for the GPS IIF program and modification for the RAFSMOD program. In: Proceedings of the 2008 IEEE International frequency control symposium, IEEE Press, Piscataway, NJ, USA, pp 655–660
- Formichella V, Camparo J, Tavella P (2017) Influence of the ac-Stark shift on GPS atomic clock timekeeping. *Appl Phys Lett* 110:043506
- Heavner TP, Barlow S, Weiss MA, Ashby N, Jefferts SR (2011) A laser-cooled frequency standard for GPS. In: Proceedings of the ION ITM 2010, Institute of Navigation, Nashville, TN, USA, 2946–2949
- Heng L, Gao GX, Walter T, Enge P (2012) Statistical characterization of GPS Signal-In-Space errors. In: Proceedings of the ION ITM 2011, Institute of navigation, Nashville, TN, USA, pp 312–319
- Hoffman-Wellenhof B, Lichtenegger H, Collins J (1993) *Overview of GPS. GPS theory and practice*, vol 2. Springer, New York, pp 13–22
- Jaduszliwer B, Huang M, Camparo J (2015) Buffer gas consumption in rubidium discharge lamps. In: Proceedings of the 2015 joint conference of the IEEE international frequency control symposium and the European frequency and time forum, IEEE, Piscataway, NJ, USA, pp 37–46
- Kasevich MA, Riis E, Chu S, DeVoe RG (1989) RF spectroscopy in an atomic fountain. *Phys Rev Lett* 63:612–615
- Kastler A (1957) Optical methods of atomic orientation and of magnetic resonance. *J Opt Soc Am* 47:255–265
- Kleppner D, Berg HC, Crampton SB, Ramsey NF, Vessot RFC, Peters HE, Vanier J (1965) Hydrogen-maser principles and techniques. *Phys Rev A* 138:972–983
- LaLumondiere SD, Moss SC, Camparo JC (2003) A “space experiment” examining the response of a geosynchronous quartz crystal oscillator to various levels of solar activity. *IEEE Trans Ultrason Ferroelectr Freq Control* 50:210–213
- Lemke ND, Phelps G, Burke JH, Martin K, Bigelow MS (2017) The optical rubidium atomic frequency standard at AFRL. In: Proceedings of the 2017 joint conference of the European frequency and time forum and the IEEE international frequency control symposium, IEEE, Piscataway, NJ, USA, pp 466–467
- Lemond P et al (1997) A space clock prototype using cold cesium atoms. In: Proceedings of the 1997 IEEE International frequency control symposium, IEEE, Piscataway, NJ, USA, pp 213–218
- Levi F, Calosso CE, Godone A, Micalizio S (2013) Pulsed optically pumped Rb clock: a high stability vapor cell frequency standard. In: Proceedings of the 2013 joint conference of the IEEE international frequency control symposium and the European frequency and time forum, IEEE, Piscataway, NJ, USA, pp 599–605
- Li J, Zhang J, Bu Y, Cao C, Wang W, Zheng H (2016) Space Passive Hydrogen maser: a passive hydrogen maser for space applications. *Proc. 2016 IEEE International frequency control symposium*, IEEE press, Piscataway, NJ, USA, pp 1–5
- Liu H, Chen Y, Yan B, Liu G, She L (2020) Progress towards a miniaturized mercury ion clock for space application. In: Sui J, Xie J (eds) *China satellite navigation conference (CNSC) 2020 Proceedings*, Vol II, pp 557–561
- Liu L et al (2018) In-orbit operation of an atomic clock based on laser-cooled ⁸⁷Rb atoms. *Nat Commun* 9:2760
- Lutwak R, Emmons D, Garvey RM, Vlitas P (2001) Optically pumped cesium-beam frequency standard for GPS-III. In: Proceedings of the 33rd annual precise time and time interval (PTTI) Meeting, pp 19–32

- Lv Y, Geng T, Zhao Q, Liu J (2018) Characteristics of BeiDou experimental satellite clocks. *Remote Sensing* 10:1847–1859
- Maciuk K (2019) Monitoring of Galileo on-board oscillators variations, disturbances and noises. *Measurement* 147:106843–106849
- Major FG (1998) *The quantum beat: the physical principles of atomic clocks*. Springer, New York
- Mei G, Zhong D, An S, Zhao F, Qi F, Wang F, Ming G, Li W, Wang P (2016) Main features of space rubidium atomic frequency standard for beidou satellites. In: *Proceedings 2016 European frequency and time forum (EFTF)*, pp 1–4
- Millerioux Y, Touhari D, Hilico L, Clairon A, Felder R, Biraben F, de Beauvoir B (1994) Towards an accurate frequency standard at $\lambda = 778$ nm using a laser diode stabilized on a hyperfine component of the Doppler-free two-photon transitions in rubidium. *Opt Commun* 108:91–96
- Montenbruck O, Steinberger P, Hauschild A (2020) Comparing the ‘Big 4’—A user’s view on GNSS performance. In: *Proceedings of the IEEE/ION PLAN 2020*, Institute of Navigation, Nashville, TN, USA, to be published
- Paul W, Osberghaus O, Fischer E (1958) *Ein Ionenkäfig*. Forschungsberichte des Wirtschafts- und Verkehrsministerium Nordrhein-Westfalen Nr 415, Westdeutscher Verlag, Cologne
- Phelps G, Lemke N, Erickson C, Burke J (2018) Compact optical clock with 5×10^{-13} instability at 1 s. *Navigation* 65:49–54
- Prestage JD, Dick GJ, Maleki L (1989) New ion trap for frequency standard applications. *J Appl Phys* 66:1013–1017
- Ramsey NF (1956) *Molecular beams*. Oxford University Press, Oxford
- Revnivkyh I (2016) GLONASS Programme update. 11th Meeting of the International Committee on Global Navigation Satellite System
- Riley WJ (2008) Time domain stability. *Handbook of frequency stability analysis*, NIST special publication 1065. US Government Printing Office, Washington DC, pp 9–66
- Rochat P (2016) Latest Evolutions on clocks & on board timing. Spectratime presentation at the Galileo Evolution Industry Days, ESA-ESTEC Noordwijk, the Netherlands, 24–25 May 2016
- Schmeissner R et al (2017) Optically pumped Cs space clock development. In: *Proceedings of the 2017 Annual IEEE frequency control symposium*, IEEE, Piscataway, NJ, USA, pp 136–137
- Shen Q, Lin H, Deng J, Wang Y (2020) Optically pumped atomic clock with a medium to long-term frequency stability of 10^{-15} . *Rev Sci Instrum* 91:045114
- Sinclair LC, Deschenes JD, Sonderhouse L, Swann WC, Khader IH, Baumann E, Newbury NR, Coddington I (2015) A compact optically-coherent fiber frequency comb. *Rev Sci Instrum* 86:081301
- Tjoelker RL, Burt EA, Chung S, Hamell RL, Prestage JD, Tucker B, Cash, P, Lutwak R (2011) Mercury atomic frequency standards for space based navigation and timekeeping. In: *Proceedings of the 2011 Precise Time and Time Interval (PTTI) Systems and Applications Meeting*, pp 293–303
- Tjoelker RL et al (2016) Mercury ion clock for a NASA technology demonstration mission. *IEEE Trans Ultrason Ferroelectr Freq Control* 63:1034–1043
- Vannicola F, Beard R, White J, Senior K, Largay M and Buisson J (2010) GPS Block IIF atomic frequency standard analysis. In: *Proceedings of the 42nd annual precise time and time interval*

- (PTTI) systems and applications meeting, Institute of Navigation, Nashville, TN, USA, pp. 181–195
- Volk CM, Frueholz RP, English TC, Lynch TJ, Riley WJ (1984) Lifetime and reliability of rubidium discharge lamps for use in atomic frequency standards. In: *Proceedings of the 38th Annual Frequency Control Symposium*, IEEE Press, Piscataway, NJ, USA, pp 387–400

Publisher’s Note Springer Nature remains neutral with regard to jurisdictional claims in published maps and institutional affiliations.



Bernardo Jaduszliwer, Lic. en Ciencias Físicas (1968), Universidad de Buenos Aires; M.Sc. (1971) and Ph.D. (1973), University of Toronto. After a year in Toronto continuing his research on positron–atom scattering, he joined the New York University Atomic Beams Laboratory as a Postdoctoral Fellow, where he conducted research in electron–atom and electron–polar molecule scattering, laser–atom interactions and atomic and molecular polarizabilities. He left NYU in 1985 as an Associate Research Professor to join the Aerospace Corporation, where he worked on atomic clocks and photonic systems for space applications. He was promoted to progressively more responsible management positions and retired in 2012 as the Principal Director of the Electronics and Photonics Laboratory. After retirement, he continues to support the GPS Program on atomic clock-related issues.



James Camparo joined The Aerospace Corporation’s Atomic Physics section in January 1981 immediately after obtaining his doctorate from Columbia University. His dissertation dealt with “laser snow” (i.e., photochemically produced cesium hydride) and the spin-exchange detection of free hydrogen/deuterium atoms created in the laser snow process. He is currently a Fellow in Aerospace’s Physical Sciences Laboratories, where his interests include research and development of the laser-pumped atomic clock, the study of atomic timekeeping onboard spacecraft, and experiments investigating the field/atom interaction.